Estimation of dispersive properties of encapsulation tissue surrounding deep brain stimulation electrodes in the rat

Author List: Karthik Sridhar, Judith Evers, Diego Pereira Botelho and Madeleine M. Lowery

Corresponding Author: Madeleine Lowery
School of Electrical and Electronic Engineering,
University College Dublin, Belfield, Dublin 4, Ireland
madeleine.lowery@ucd.ie

Affiliations: J Sridhar, J Evers, D Pereira Botelho and M. M. Lowery are with the School of Electrical and Electronic Engineering, University College Dublin, Ireland.

Link to Published Manuscript, DOI: 10.1109/EMBC.2019.8857062

Details of Funding: Research supported by Science Foundation Ireland (SFI), the European Regional Development Fund (Grant Number: 13/RC/2073) and the European Research Council (Grant Number: ERC-2014-CoG-646923- DBSModel).

Abstract

The aim of this study was to estimate the electrical properties of the encapsulation tissue surrounding chronically implanted electrodes for deep brain stimulation in the rat. The impedance spectrum of a concentric bipolar microelectrode implanted in the rat brain was measured immediately following surgery and after 8 weeks of implantation. The experimental impedance data were used in combination with a finite element model of the rat brain using a parametric sweep method to estimate the electrical properties of the tissue surrounding the electrode in acute and chronic conditions. In the acute case, the conductivity and relative permittivity of the peri-electrode space were frequency independent with an estimated conductivity of 0.38 S/m and relative permittivity of 123. The electrical properties of the encapsulation tissue in the chronic condition were fitted to a dispersive Cole-Cole model. The estimated conductivity and relative permittivity in the chronic condition at 1 kHz were 0.028 S/m and 2×10^5, respectively. The estimated tissue properties can be used in combination with computational modeling as a basis for optimization of chronically implanted electrodes to increase the efficacy of long-term neural recording and stimulation.

Introduction

Over the past twenty years, deep brain stimulation (DBS) has been established as an effective clinical intervention to restore motor function in patients with Parkinson's disease. However, the mechanisms by which it works are not yet fully understood. To better understand the mechanisms of DBS it is necessary to establish the distribution of the electric field induced in the surrounding tissues and the effect that it has on activity in the target neurons. Mathematical modelling has been widely used to investigate the electric field distribution and consequent volume of neural tissue activated [1], [2], [16]. Using this approach, bioelectric field modelling of the brain has been extensively used for surgical planning, and to investigate variations in electrode configuration and simulation parameters system [1], [19]. Accurate modelling of the electric field requires knowledge of the distinctive properties of the electrode-tissue interface which includes the electrical double layer formed at the electrode-tissue interface and the electrical and geometrical properties of the encapsulation tissue formed around the electrodes. The electrical properties of the encapsulation layer are poorly understood and vary widely in the reported values used in the literature. Since the accuracy of computational models of DBS in predicting realistic electric fields directly depends on electrical properties and representation of anatomical structures of the tissues in the brain, identification of these properties is a critical issue. The encapsulation tissue formed at the electrode-tissue interface can have a substantial effect on the region of tissue which is stimulated. During voltage controlled stimulation, the

54 electric field in the surrounding tissues reduces significantly due to an increase of the impedance
55 at the electrode-tissue interface resulting from the formation of a glial scar. In the chronic
56 condition, the impedance of the encapsulation tissue increases for several weeks after
57 implantation and remains while the implant is in the body. It is also reported that both
58 encapsulation tissue properties and the thickness of the layer may change over time [3]. In the
59 context of computational modelling of DBS, incorporation of the electrical double layer at the
60 electrode tissue interface is well-established [4]. However, models to date have considered the
61 encapsulation tissue to be purely resistive and frequency independent [5], [2], [17]. It has been
62 established that capacitive and dispersive properties of the surrounding brain tissue can
63 influence the volume of tissue activated during deep brain stimulation [2], [7]. However, it is
64 not clear whether the encapsulation tissue exhibits similar capacitive or dispersive. The aim of
65 the present study was, therefore, to estimate the electrical double layer and electrical properties
66 of encapsulation tissue surrounding a DBS electrode chronically implanted in the rat brain,
67 across a range of frequencies. The estimated electrode-tissue properties were incorporated in a
68 computational finite element model of the electrode and surrounding brain tissue.

Methods

In this study, experimentally recorded impedance data were used in combination with a three-dimensional heterogeneous finite element (FE) model of the rat brain to estimate dispersive properties of the encapsulation tissue surrounding an implanted DBS electrode. Tissue properties were estimated in both acute and chronic conditions, on the day of surgery and eight weeks after surgery, respectively, in the frequency range of 100 Hz to 30 kHz.

A. Impedance measurement in vivo

Electrochemical Impedance Spectroscopy (EIS) was performed on the microelectrode in both physiological saline and then in the brain of one male adult Wistar rat in vivo, using Keysight E4980 AL precision LCR (inductance (L), capacitance (C), and resistance (R)) meter and Keysight data acquisition software (Keysight Technologies, CA, USA). Impedance was measured between the frequency range of 20 Hz to 300 kHz by applying a single sinusoidal signal of 20 μA in amplitude. The SNEX-100 concentric bipolar electrode (Microprobes, Gaithersburg, USA) was used with active Platinum/Iridium electrode contact with a diameter of 100 μm and stainless steel ground contact with a diameter of 310 μm. The experiments were approved by the UCD Animal Ethics Committee and licensed by the Health Products Regulatory Authority of Ireland.

B. Impedance data analysis

To estimate the equivalent circuit electrical double layer (EDL) parameters, a circuit model similar to that proposed by McAdams and Richardot[8] was used to fit the impedance spectrum of the electrode in saline, using the simplex optimization technique in MATLAB (The MathWorks, Natick, USA). The equivalent impedance of a 1 nm thick electrical double layer was represented as a parallel combination of the constant phase angle element (Z_{cpa}) and the over potential independent form of the charge transfer resistance (R_{ct}):

$$Z_{cpa} = K(i\omega)^{-\beta} \qquad (1)$$

$$R_{ct} = \frac{RT}{nFI_0} \qquad (2)$$

where K and β are constants denoting the magnitude of Z_{cpa} and inhomogeneities in the surface respectively, R is the universal gas constant, F Faradays constant, T temperature, n the number of electrons per molecule, and I_0 the exchange current density.

C. Model geometry

A heterogeneous rat model with geometrical structures comprising cerebrospinal fluid (CSF), skull, grey and white matter tissue of the brain was created using image segmentation of T2 MRI dataset of the rat brain [10]. The segmented masks of brain tissues were converted to a geometric model using Simpleware ScanIP software (Synopsys, CA 94043, USA). Before segmentation, the MRI dataset was coregistered to Waxholm Space Atlas of the Sprague Dawley Rat Brain (WSSD) atlas[10]. Subsequently, the microelectrode was positioned on the subthalamic nucleus with the aid of WSSD atlas as shown in Fig. 1. Finally, a surrounding layer of tissue of 25 µm and 60 µm thickness was created in the geometry to represent the encapsulation layer for acute and chronic, respectively.

D. Mathematical framework

To simulate the electrode impedance at different frequencies, the electro-quasistatic equation was used, where magnetic and wave propagation effects were neglected [11], [2], [6]:

$$\nabla.[(\sigma(\omega)+i\omega\varepsilon_r(\omega)\varepsilon_0)]\nabla\phi \qquad (3)$$

where, σ (S/m) and ε_r are electrical conductivity and relative permittivity, ω - angular frequency, ε_0 permittivity of free space (F/m), and φ(Volts) scalar potential. Maxwell's equation in this form takes into account the frequency dependent conductivity and permittivity, where both conductivity and permittivity were described using the Cole-Cole model representation [15].

E. Boundary conditions and material properties

For bipolar stimulation in the computational model, the Platinum-iridium (Pt/Ir) contact of the microelectrode was assigned as the active terminal and the stainless-steel contact as a ground. Neumann boundary conditions were applied to the insulating parts of the electrode and outer surface of the skull [2]. The estimated electrical double layer was implemented using the thin layer approximation for voltage controlled stimulation and the equivalent double layer circuit model coupled to the active terminal of the electrode for current controlled stimulation [4]. The electrical double layer properties were estimated from the in vitro impedance data of the electrode in physiological saline and the skull, grey and white matter tissue properties were obtained from [15].

F. Estimation of encapsulation tissue properties

A parametric sweep method was used where the Cole-Cole parameters of the encapsulation tissue were swept between grey matter and CSF for the acute condition, and for the chronic

condition between the white matter and 175% of the white matter properties [15]. Solving the FE model for each set of parameters, the parameters for which the deviation between the experimentally recorded and simulated impedance data, across the frequency range from 500 - 27.5 kHz, was minimized were identified. Assuming linearity at the electrical double layer interface [9], [13], the impedance of the electrode can be calculated using Ohms law:

$$Z = \frac{V}{I} \qquad (4)$$

where, Z is the magnitude of the impedance of the electrode, V - electric potential(Volts) calculated from the Laplace equation, and I - applied current (Amperes).

G. Implementation detail

The head with DBS electrode model was meshed using the Simpleware software, generated model consists of 1.8 million tetrahedral elements. A quadratic interpolation function was used on each tetrahedral element creating 2.5 million degrees of freedom to approximate the scalar potential. Finally, the discretized finite element model was solved using COMSOL Multiphysics (COMSOL, Stockholm, Sweden) using the GMRES iterative solver with a geometric multigrid preconditioner.

Results

A. Estimation of electrical properties of the double layer

The estimated impedance of the microelectrode in the 0.9 % saline was presented in Fig. 2. The estimated parameters of the constant phase angle element of equation (1) normalized with respect to the active microelectrode surface area were K = 0.96 Ωm 2 s −β , β = 0.78. The estimated charge transfer resistance Rct was 350 kΩ. The impedance due to the electrical double layer was dominant in the low frequency range up to 10 kHz.

B. Estimation of peri-electrode space electrical properties in acute phase

The estimated electrical conductivity and relative permittivity of the 25 µm thick encapsulation layer in the acute condition were 0.38 S/m and 123, respectively at 1 kHz. The estimated dispersive properties of the encapsulation tissue were found to be constant across the frequency range examined. The estimated peri-electrode space electrical properties yielded an impedance of the electrode comparable to the experimental data as shown in Fig. 3.

C. Estimation of encapsulation tissue properties in the chronic phase

The estimated electrical conductivity and relative permittivity of the 60 µm thick encapsulation layer in chronic phase were approximately 0.028 S/m and 2.5×10^5 respectively at 1 kHz. The estimated conductivity increased from 0.025 S/m to 0.081 S/m across the frequency range of 600 Hz to 27.5 kHz, whereas relative permittivity decreased from 3.5×10^5 to 5.7×10^4 . The estimated dispersive properties were in close agreement with the experimental results as shown in Fig. 4.

Discussion

In this study, the dispersive electrical properties of the encapsulation tissue surrounding an implanted microelectrode in the rat brain were estimated using a 3D finite element model. Encapsulation tissue properties were estimated for both acute and chronic conditions. Before estimating the encapsulation tissue properties, the electrical double layer impedance was first estimated in vitro. The electrical double layer was then incorporated in the FE models to estimate the encapsulation tissue properties in both the acute and chronic conditions. In both conditions, the electrical double layer impedance was dominant in the low frequency range(see Fig. 3 and Fig. 4), and was consistent with values estimated previously for DBS electrodes in a non-human primate [14].

In the acute condition, the estimated electrical properties of the peri-electrode space were frequency independent, and the influence of permittivity on the electrode impedance was negligible, as shown in Fig. 3. A single conductivity value for the encapsulation produced a comparable impedance spectrum to the *in vivo* impedance data (see Fig. 3). The surrounding tissue conductivity of 0.38 S/m estimated on the day of surgery was found to be substantially lower than the values for CSF (1.7-2 S/m) which are frequency independent used as the basis for simulation of peri-electrode space properties in the acute phase [2], [5], [18]. The difference in the electrical conductivity in the peri-electrode space from that of CSF may be due to the presence of other cells resulting from insertion of the microelectrode. The conductivity estimated here lies above the effective conductivity of 0.1-0.27 S/m for a suspension of cell bodies within CSF reported in [12].

In the chronic condition, the estimated electrical properties of the encapsulation tissue were frequency dependent, and the permittivity had a substantial influence on the impedance for the measured frequency range. The impedance simulated assuming a single value of conductivity and relative permittivity for the encapsulation tissue was not able match the *in vivo* impedance data (see Fig. 4). The estimated conductivity of the encapsulation tissue of 0.038 S/m at 1 kHz

is higher than that reported previously for subcutaneously implanted epoxy and silicone rubber electrode arrays in the cat [17]. Variations in the impedance values observed across the studies are likely due to differences in the tissue in which the electrodes were implanted, variations in materials and in electrode geometry. A number of study limitations should be considered when interpreting the data. The preliminary data presented were recorded in a single rat. A group study is ongoing to quantify the variability across animals. The electrical properties of the double layer were estimated *in vitro* and may change slightly *in vivo* and over time. Finally, the encapsulation tissue was assumed to be a homogenous isotropic conductor of simplified geometrical structure. The estimated electrical properties thus represent macroscopic bulk tissue properties. The detailed structure of glial scar and variations in tissue with distance from the electrode may influence the distribution of the electrode field in the region immediately surrounding the electrode in computational volume conductor models.

Conclusions

A detailed model of the rat brain was used in combination with experimentally recorded impedance data to estimate the electrical properties of the peri-electrode space and encapsulation tissue surrounding an implanted DBS electrode in the rat. The results confirm the increase in electrode impedance in the weeks following implantation observed in previous animal and human studies, and provide an estimate of the change in corresponding electrical properties of the tissue immediately surrounding the electrode. The estimated tissue properties can be used in combination with computational modeling as a basis for optimization of chronically implanted electrodes to increase the efficacy of long-term neural recording and stimulation.

References

[1] C. R. Butson, C. B. Maks, C. C. McIntyre, S. E. Cooper, J. M. Henderson, and C. C. McIntyre, “Patient-specific analysis of the volume of tissue activated during deep brain stimulation,” Clin. Neurophysiol., vol. 117, no. 2, pp. 661670, 2007.

[2] P. F. Grant and M. M. Lowery, “Effect of dispersive conductivity and permittivity in volume conductor models of deep brain stimulation,” IEEE Trans. Biomed. Eng., vol. 57, no. 10 PART 1, pp. 23862393, 2010.

[3] S. F. Lempka, S. Miocinovic, M. D. Johnson, J. L. Vitek, and C. C. McIntyre, “In vivo impedance spectroscopy of deep brain stimulation electrodes,” J. Neural Eng., vol. 6, no. 4, 2009.

[4] D. R. Cantrell, S. Inayat, A. Taflove, R. S. Ruoff, and J. B. Troy, “Incorporation of the electrode-electrolyte interface into finite-element models of metal microelectrodes,” J. Neural Eng., vol. 5, no. 1, pp. 5467, 2008.

[5] N. Yousif and X. Liu, “Modeling the current distribution across the depth electrodebrain interface in deep brain stimulation,” Expert Rev. Med. Devices, vol. 4, no. 5, pp. 623631, Sep. 2007.

[6] B. Tracey and M. Williams, “Computationally efficient bioelectric field modeling and effects of frequency-dependent tissue capacitance,” J. Neural Eng., vol. 8, no. 3, 2011.

[7] C. A. Bossetti, M. J. Birdno, and W. M. Grill, “Analysis of the quasistatic approximation for calculating potentials generated by neural stimulation,” J. Neural Eng., vol. 5, no. 1, pp. 4453, 2008.

[8] A. Richardot and E. T. McAdams, “Harmonic analysis of lowfrequency bioelectrode behavior,” IEEE Trans. Med. Imaging, vol. 21, no. 6, pp. 604612, 2002.

[9] E. T. McAdams and J. Jossinet, “A physical interpretation of Schwans limit current of linearity,” Ann. Biomed. Eng., vol. 20, no. 3, pp. 307319, 1992.

[10] E. A. Papp, T. B. Leergaard, E. Calabrese, G. A. Johnson, and J. G. Bjaalie, “Waxholm Space atlas of the Sprague Dawley rat brain,” Neuroimage, vol. 97, pp. 374386, 2014.

[11] N. S. Stoykov, M. M. Lowery, A. Taflove, and T. A. Kuiken, “Frequency- and time-domain FEM models of EMG: Capacitive effects and aspects of dispersion,” IEEE Trans. Biomed. Eng., vol. 49, no. 8, pp. 763772, 2002.

243 [12] C. Gabriel, A. Peyman, and E. H. Grant, “Electrical conductivity of tissue at frequencies
244 below 1 MHz,” Phys. Med. Biol., vol. 54, no. 16, pp. 48634878, 2009.

245 [13] B. Onaral and H. P. Schwan, “Linear and nonlinear properties of platinum electrode
246 polarisation. Part 1: frequency dependence at very low frequencies,” Med. Biol. Eng. Comput.,
247 vol. 20, no. 3, pp. 299306, 1982.

248 [14] S. F. Lempka, S. Miocinovic, M. D. Johnson, J. L. Vitek, and C. C. McIntyre, “In vivo
249 impedance spectroscopy of deep brain stimulation electrodes,” J. Neural Eng., vol. 6, no. 4,
250 2009.

251 [15] S. Gabriel, R. W. Lau, and C. Gabriel, “Physics in Medicine Biology. The dielectric
252 properties of biological tissues: III. Parametric models for the dielectric spectrum of tissues,”
253 Phys. Med. Biol. Phys. Med. Biol, vol. 41, no. 41, pp. 22512269, 1996.

254 [16] M. Astrom, E. Diczfalusy, H. Martens, and K. W ¨ ardell, “Relationship ¨ between neural
255 activation and electric field distribution during deep brain stimulation,” IEEE Trans. Biomed.
256 Eng., vol. 62, no. 2, pp. 664672, 2015.

257 [17] W. M. Grill and J. Thomas Mortimer, “Electrical properties of implant encapsulation
258 tissue,” Ann. Biomed. Eng., vol. 22, no. 1, pp. 2333, 1994.

259 [18] A. R. Kent and W. M. Grill1, “Analysis of deep brain stimulation electrode characteristics
260 for neural recording,”vol. 71, no. 11, pp. 38313840, 2014.

261 [19] C. R. Butson, J. Vorwerk, A. D. Dorval, D. N. Anderson, and B. Osting, “Optimized
262 programming algorithm for cylindrical and directional deep brain stimulation electrodes,” J.
263 Neural Eng., vol. 15, no. 2, p. 026005, 2017.

264

Figures

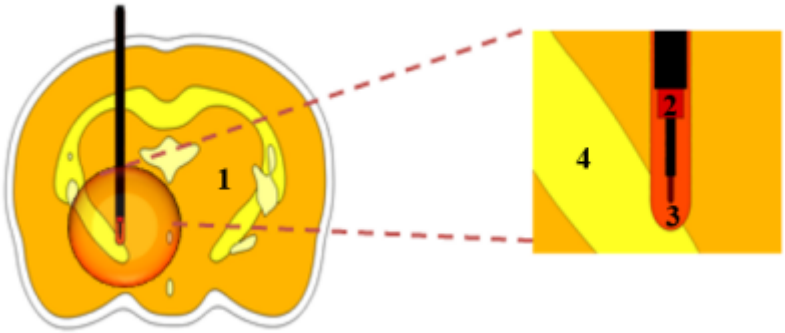

Fig. 1. Cross sectional view of model of rat brain with micro electrode, where 1-Grey matter, 2-micro-electrode, 3-encapsulation tissue, 4-white matter

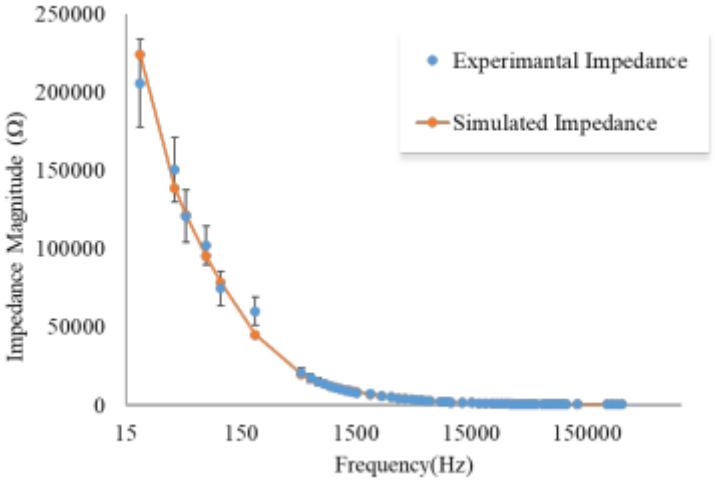

Fig. 2. Comparison of experimentally measured electrode impedance and electrode impedance estimated for the FE model in 0.9% saline.

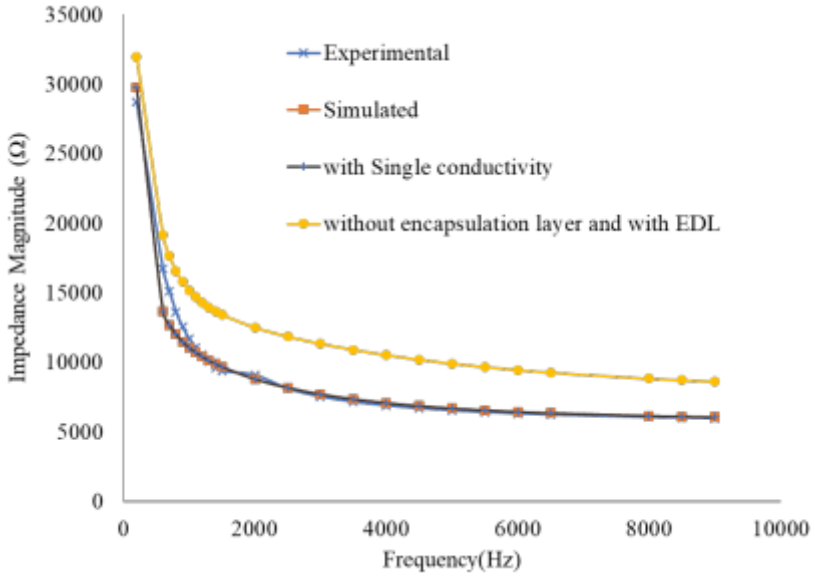

278

279

280 **Fig. 3**. Comparison of experimentally measured electrode impedance and electrode impedance
281 estimated for the FE model in the acute condition. Data are also shown for the FE model where
282 the electrical double layer (EDL) was included but the peri-electrode space was omitted from
283 the model.

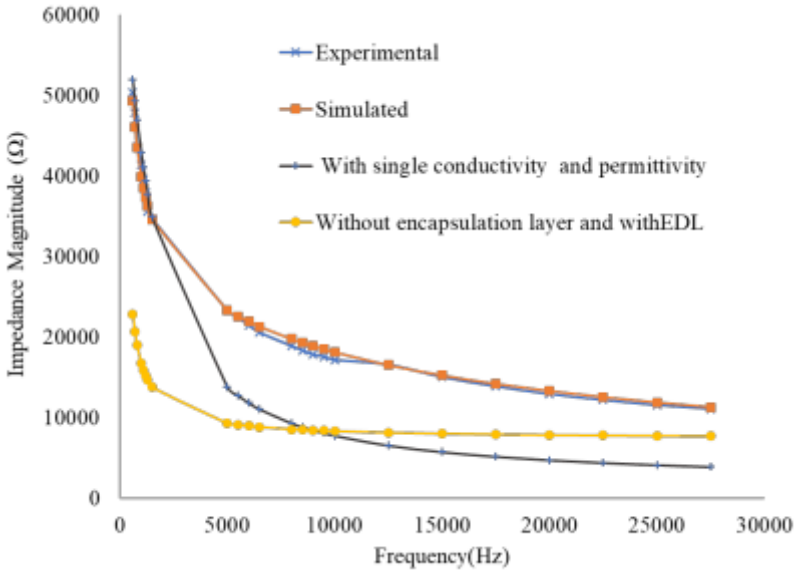

284

285 **Fig. 4.** Comparison of experimentally measured electrode impedance and electrode impedance
286 estimated for the FE model in the chronic condition. Data are also shown for the FE model
287 where the electrical double layer (EDL) was included but the encapsulation tissue was removed
288 from the model and for conductivity and relative permittivity values estimated at a single
289 frequency.